METALS AND MATERIALS International, Vol. 8, No. 5 (2002), pp. 469~477

Effect of Dilution on the Behavior of Solidification Cracking in PTAW Overlay Deposit on Ni-Base Superalloys

Yongsoo Ahn, Byunghyun Yoon*, Hyungjun Kim*, and Changhee Lee

Division of Materials Science and Engineering, Hanyang University
17 Haengdang-dong, Seongdong-gu, Seoul 133-791, Korea
*Research Institute of Industrial Science and Technology
San 32 Hyoja-dong, Nam-gu, Pohang 790-600, Korea

In this study, the effects of dilution on the solidification cracking susceptibility of PTAW (Plasma Transferred Arc Welding) Inconel 625 and 718 overlay on Nimonic 80A were observed. In order to evaluate solidification cracking susceptibility, the Varestraint test was utilized. A possible mechanism of solidification cracking was suggested on the basis of microstructural examination and thermal analysis. The present study showed that the solidification cracking of the diluted Inconel 625 and 718 with Nimonic 80A was closely related to the solidification temperature range and the amount and distribution of γ/NbC and γ/Laves eutectic phases formed along the solidification grain boundaries. As dilution increased, the C/Nb ratio increased and the amount of eutectic phases decreased. In addition, the solidification temperature range decreased with increasing dilution in each overlay.

Keywords : plasma transferred Arc welding (PTAW), Inconel 625 and 718, Varestraint test, solidification cracking susceptibility, γ/NbC and γ/Laves eutectic phases

1. INTRODUCTION

In conventional exhaust valve spindles, the materials primarily used are heat resistant Nimonic 80A having a Stellite 6 alloy deposited over it [1-3]. However, there are cost problems associated with the use of Stellite 6 alloy overlayed with PTAW (Plasma Transferred Arc Welding) on Nimonic 80A exhaust valve spindles. This is particularly apparent in large diesel engines, for which large exhaust valves are required. In addition, increasing demand for improved performance in engines will inevitably bring further elevated costs. So, recently, the Inconel 625 and 718 are being substituted for Stellite 6 because of similar hot corrosion resistance with Stellite 6 and lower costs. However, hot cracking occurs in PTAW Ni-base superalloys overlay. The effect of hot cracks on the overlay performance will generally depend on the degradation mechanism that is operable. Small cracks generally do not compromise the overlay integrity. In corrosion applications, hot cracks will be detrimental if they traverse through the entire overlay thickness, in which case they will provide a path for aggressive gases to reach the underlying substrate. Therefore hot cracking must be controlled in the PTAW Ni-base superalloys overlay.

Weld metal solidification cracking occurs during the final stages of solidification due to the inability of the nearly solidified weld metal to accommodate thermal and/or mechanical restraint stresses [4]. The main factors that control solidification cracking susceptibility are the solidification temperature range and type of interfacial liquid that exists at the last stages of solidification. Solute element segregation affects the solidification temperature range and the amount of the low melting eutectic phase [4-10]. In austenitic high alloys (Inconel 625 and 718) that contain Nb, Mo and Ti, non-equilibrium solidification in the weld region promotes the partitioning of these elements to the last to solidify the interdendritic regions [11]. This segregation extends the alloy solidification range and promotes final solidification to a low melting point, Nb-rich eutectic. Both the increase in solidification temperature range and partitioning of melting point depressant elements such as Nb and Ti have been shown to increase susceptibility to solidification cracking in Ni-base alloys.

When a coating of dissimilar materials is overlayed on the substrate in PTAW, dilution between overlay and substrate inevitably occurs. Therefore, the chemical mixing causes the resultant microstructure to change. The solidification cracking susceptibility of Inconel 625 and 718 overlays depends strongly on the microstructures. Small changes in Nb, Mo, Ti and C influence the final solidification temperature, type and amount of precipitation phases and resultant solidifica-

tion cracking susceptibility. In Inconel 625 and 718 overlays, it has been known that two types of eutectic type constituents, γ/NbC and γ/Laves, are formed. [5,6] The g/Laves eutectic phase forms at a lower temperature and expands the solidification temperature range. Therefore, it is most deleterious in hot cracking.

In this study, the effect of composition change with dilution on solidification cracking and the mechanism of formation and propagation of solidification cracking are discussed for the PTAW Inconel 625 and 718 overlays. In additional, the critical phase balance (γ/NbC and γ/Laves) with chemistry is discussed.

2. EXPERIMENTAL PROCEDURES

2.1. Experimental alloy compositions

Inconel 625 and 718 powders were deposited on Nimonic 80 A which is used in the exhaust valve spindle using PTAW. The compositions of the alloys used in this study are given in Table 1. To observe the variation in composition in the layer and the behavior of solidification cracking with dilution, Inconel 625 and 718 PTAW overlays were formed with 10%, 20% and 30% dilution by controlling the powder feed rate. Table 2 shows the chemical composition of the specimens after PTA overlay welding. In the figure, D indicates the percentage of dilution.

2.2. Varestraint testing

The solidification cracking susceptibility of the Inconel 625 and 718 layers was evaluated using Varestraint testing [12,13]. The overlay samples were machined to typical subsize Varestraint specimens (165×25×3.2 mm). A schematic representation of the Varestraint test and specimen are displayed in Fig. 1. The welds were produced under the following parameters: 80 A, 2 mm arc distance, and 500 mm/min travel speed with argon shielding. In this test, straining occurs as a moving GTA weld is made with cracks forming in the nearly solidified weld fusion zone at the trailing edge of the molten weld pool. The augmented strain imparted to the outer surface of the test specimen during the Varestraint tests is approximated by the relationship:

$$\varepsilon = t/2R$$

where t is the thickness of the sample and R the radius of the die block. In this study, augmented strains of 1% and 4% were applied. Duplicated tests were conducted for each alloy at individual dilution. Quantitative cracking data for both tests were obtained by measuring the length of each crack on the as-tested surface using low-magnification optical microscopy at a magnification of x25. Total crack length (TCL) and maximum crack length (MCL) were recorded for each sample.

2.3. Metallurgical characterization

The Varestraint test specimens were metallographically prepared by sectioning, mounting in epoxy, grinding and polishing through 0.05 micron alumina. Microstructural details were revealed by electro-etching with a 10% chromic acid + 90% water solution at 3 V. Characterization methods included light and scanning electron microscopy and energy-dispersive x-ray analysis. In order to confirm the mechanism of the solidification cracking process, regions of Varestraint test samples containing cracks were carefully sectioned and then fractured to reveal the crack surfaces for fractographic analysis using SEM.

2.4. Differential thermal analysis

In order to examine the solidification temperature range of each alloy, differential thermal analysis was conducted using differential scanning calorimeter (DSC). The samples were melted and solidified under flowing argon in alumina crucibles using pure Ni as the reference material. The specimen was heated to 1400°C, and the heating and cooling rates

Table 1. The chemical compositions of the alloys used in this study (unit: wt.%)

	Ni	Cr	Fe	Ti	Nb	Mo	C	Si
Nimonic 80A	76.38	17.57	1.43	2.50	-	-	0.070	0.016
Inconel 625	63.57	19.76	2.74	0.10	3.56	8.50	0.058	0.480
Inconel 718	54.45	17.71	17.37	1.01	4.97	2.93	0.045	0.200

Table 2. Chemical compositions of Inconel 625 and 718 layer with various dilution after PTA welding (unit: wt.%)

	Ni	Cr	Fe	Ti	Nb	Mo	C	Si
Inconel 625 D10	64.60	19.91	2.70	0.13	3.59	8.53	0.059	0.475
Inconel 625 D20	66.79	20.52	2.31	0.55	2.82	6.59	0.060	0.409
Inconel 625 D30	67.38	20.62	2.26	0.74	2.75	6.34	0.067	0.351
Inconel 718 D10	58.71	17.43	16.38	1.09	4.47	2.61	0.049	0.203
Inconel 718 D20	59.09	18.09	14.88	1.33	3.99	2.51	0.053	0.179
Inconel 718 D30	63.84	18.18	11.87	1.55	3.47	1.89	0.058	0.130

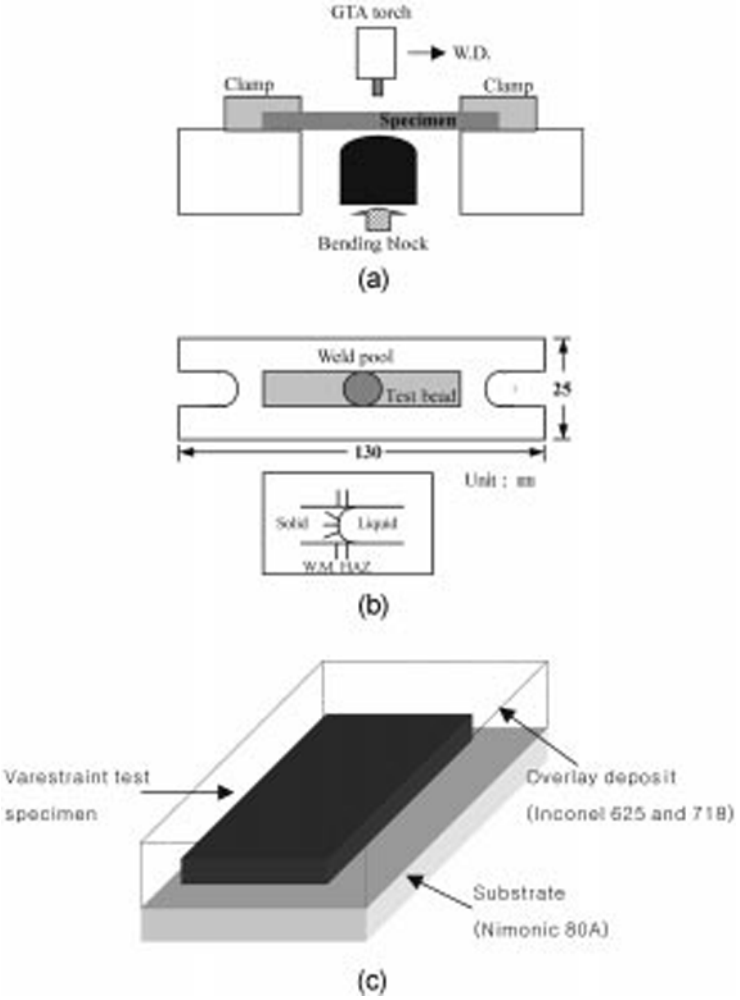

Fig. 1. Schematic diagrams of Varestraint test and specimen preparation: (a) Schematic diagram of Varestraint test; (b) Varestraint test specimen; and (c) Overlay samples for Varestraint test.

were 10°C/min. During cooling, a major peak of g matrix and 2 minor peaks related to eutectic-type reactions were observed. Reaction temperatures were taken as deviations from the local baseline.

3. RESULTS AND DISCUSSION

3.1. Macroscopic cracking characteristics

Fig. 2 shows typical macroscopic fusion zone solidification cracks in an Inconel 718 varestraint specimen tested at 4% augmented strain. Intergranular cracks were observed to emanate radially outward from the location of the trailing edge of the weld pool at the instant of straining. In Fig. 2, the large arrow indicates the instantaneous solid-liquid interface at the instant of straining and the small arrow indicates the fusion boundary. The solidification crack propagation was primarily normal to the trailing edge of the weld pool. At a higher magnification of the SEM micrograph of the fusion zone solidification crack (Fig. 3), the dendritic solidification substructure and the intergranular nature of the crack are observed.

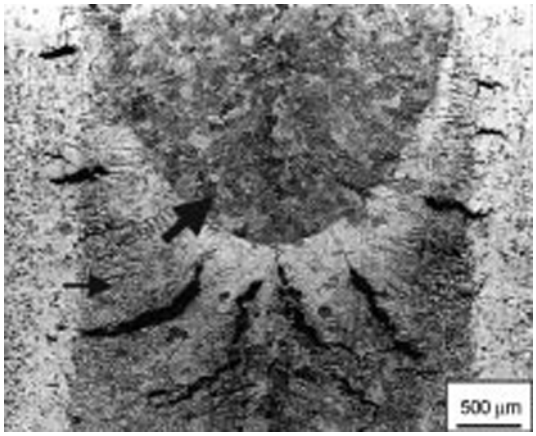

Fig. 2. Light macrograph showing the top surface of an Inconel 718 Varestraint specimen tested 4% augmented strain.

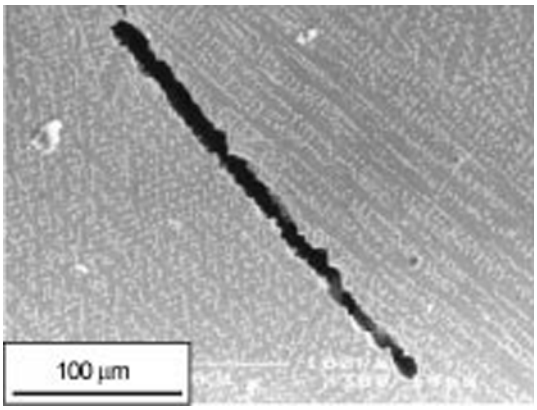

Fig. 3. SEM micrographs of a fusion zone solidification cracks in an Inconel 718 Varestraint test specimen.

3.2. Quantitative cracking analysis

In this study, maximum crack length (MCL) and total crack length (TCL) were used for evaluation and comparison of the solidification cracking susceptibilities of Inconel 625 and 718 overlay deposits with various dilutions (10%, 20% and 30%). The TCL and MCL for each overlay deposit are presented in Fig. 4.The TCL and MCL progressively decreased with the increase in dilution. The solidification cracking susceptibility of Inconel 718 overlays is noticeably greater than that of Inconel 625 overlays. Inconel 718 D10 overlay has the greatest cracking susceptibility. As discussed in detail later, these changes in solidification cracking susceptibilities with dilution are closely related with the Nb and Mo contents in the alloy. As dilution increased, the Nb and Mo content of the overlays decreased. As Inconel 718 has a higher contents of these elements than Inconel 625, the decrease in cracking susceptibility can be predicted by the decrease in Nb and Mo content.

3.3. Microstructure characterization

Solidification of the fusion zone for Inconel 625 and 718 overlay deposits occurred in the g-austenite in a cellular-dendritic mode. The partitioning of Nb, Mo and Ti in the dendrite interstices during solidification (*i.e.*, partition coefficient, k<1) promoted appreciable compositional variations in the solidification grain and substructural boundaries and the formation of terminal eutectic constituents (γ/NbC and γ/Laves) in the last-to-solidify regions [7-12]. The formation of the g/Laves constituent results in a substantial suppressing of the final solidification temperature. Thus, the cracking tendency of the overlay deposits is connected with these eutectic constituents, especially, the γ/Laves eutectic phase.

Typical solidification microstructures of the overlay are presented in Fig. 5. These SEM photographs were taken in the vicinity of solidification cracks produced during the Varestraint test. In addition to primary austenite dendrites, the alloys form eutectic type constituents during solidification. Fig. 6 presents a SEM photograph of the solidification crack tip and EDS analysis of each phase. The crack coincided with second phases located at the grain boundary. Figs. 6(b) and (c) indicate that the second phase is enriched in elements of high atomic number (*e.g.*, Nb and Mo) relative to the matrix. Fig. 7 shows an EDS analysis conducted across several dendrites within the overlay deposit. The positions of the interdendritic region are marked with ID. The matrix forming elements (*i.e.*, Ni, Cr, and Fe) are slightly depleted and the solute elements (Nb, Mo and Ti) were enriched in the interdendritic region. Nb especially was highly enriched in the dendrite boundaries. Table 3 presents the composition of the γ matrix and γ/Laves constituents in Inconel 625 and 718. The Nb and Mo contents in the γ/Laves constituent are higher than that of the g matrix. As stated, Nb, Mo and Ti are partitioned to interdendritic regions and are generally found at greater concentrations in the γ/Laves constituent than in either the bulk composition or the γ matrix.

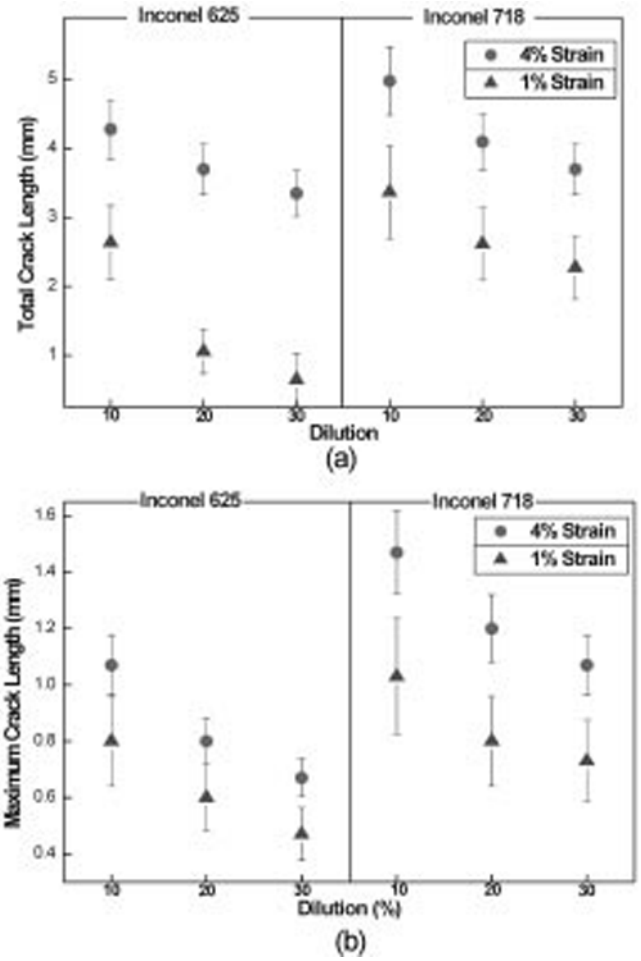

Fig. 4. Comparison of fusion zone solidification cracking susceptibility of alloys: (a) Total crack length (TCL); and (b) Maximum crack length (MCL).

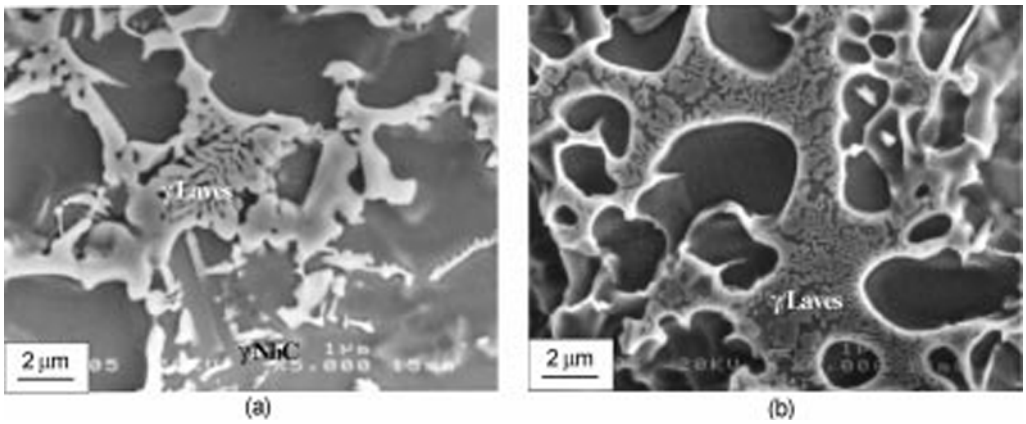

Fig. 5. Solidification microstructures of the weld metal in the vicinity of solidification cracks: (a) Inconel 625 overlay deposit; and (b) Inconel 718 overlay deposit.

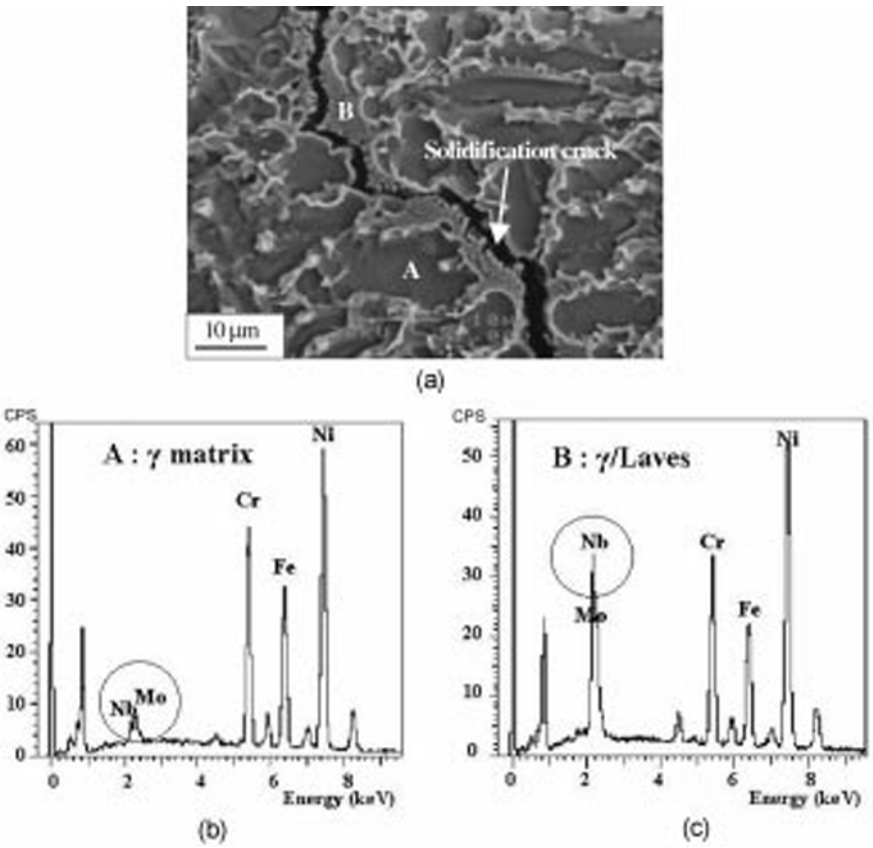

Fig. 6. Typical fusion zone solidification crack in (a) Inconel 718, and (b), (c) EDS analysis.

The role of the segregation phenomena is extremely important when considering solidification and the cracking susceptibility of the Inconel 625 and 718 alloys.[5] The solidifying dendrites are enriched or depleted in solute depending on the primary solidification phase and the partition coefficient, k, for each element. This enrichment is responsible for the formation of the γ/Laves and γ/NbC eutectics which form at the last stage of the solidification.

3.4. Critical phase balance with chemistry

The relative amounts of γ/NbC and γ/Laves phase control the solidification cracking susceptibility of the overlay deposits. Therefore, the relationship between dilution and relative phase fractions of γ/NbC and γ/Laves have to be considered as shown in Fig. 8. The amount of total eutectic constituents (γ/NbC and γ/Laves) decreases with increasing dilution. As dilution increases, the amount of γ/NbC increases while γ/

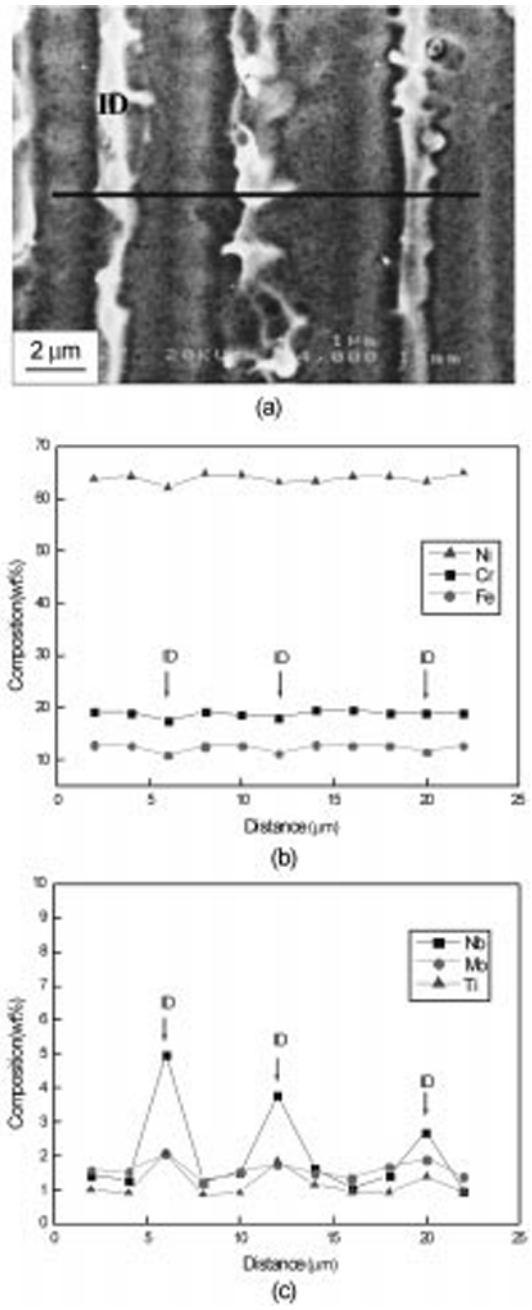

Fig. 7. Concentration profiles of Ni, Cr, Fe, Nb, Mo and Ti across the dendrite in Inconel 718: (a) SEM image; (b) matrix elements; and (c) solute elements.

Laves decreases. Mo addition to the austenite matrix can promote the formation of γ/Laves, while the addition of Ti and C can promote the γ/NbC. Nb addition also promotes the amounts of the total eutectic constituent [14]. In this study, as the dilution increased in the Inconel 625 and 718 overlay deposits, Mo which is a Laves stabilizer decreased and carbide former Ti and C contents increased. Nb content decreased with increasing dilution. Thus, the decrease in the total amount of eutectic constituent could be expected.

The primary controlling factor in the formation of eutectic constituents is the C/Nb ratio. The alloys with high C/Nb ratio have a higher carbide/Laves ratio than low C/Nb ratio alloys. Table 4 represents the C/Nb ratio and the amount of eutectic constituents for each of the Inconel 625 and 718 overlay deposits. The change in the amount of eutectic constituents with C/Nb ratio is presented in Fig. 9. As the C/Nb ratio is increased, the amount of γ/NbC slightly increases and γ/Laves decreases and the amount of total eutectic constituent decreases.

The change in the phase balance with the C/Nb ratio can be explained with the solidification paths. [7,8,10,15]. The liquidus projection for the ternary Ni-Nb-C system is schematically shown in Fig. 10(a) and the solidification paths with C/Nb ratios are shown in Fig. 10(b). The primary γ dendrites form, while segregating Nb and C to the remaining liquid. When the solidification path meets with the γ/NbC line, the γ/NbC eutectic constituent forms from the liquid through a eutectic-type reaction. The formation of NbC depletes the content of C in the remaining liquid. As the solidification is completed, the remaining high Nb/C content liquids are transformed into γ/Laves eutectic phases.

As the C/Nb ratio decreased (1>2>3), the liquid becomes more highly enriched in Nb and the intersection point occurs at higher Nb contents (Fig. 10(b)). As a result, the liquid composition will follow a short distance from the γ/NbC eutectic line, and form a small amount of γ/NbC eutectic constituent. Therefore, large amounts of the liquid remaining along the dendrite boundaries were transformed into γ/Laves eutectic constituent. Therefore, a low C/Nb ratio alloy had a large amount of γ/Laves eutectic constituent.

Fig. 11 plots the total crack length as a function of the C/Nb ratio. The solidification cracking susceptibilities of the overlay deposits decreased while increasing the C/Nb ratio of the increasing dilution. The low C/Nb alloy (*i.e.*, Inconel 718 D10) had a higher solidification cracking susceptibility due to larger amounts of the γ/Laves eutectic constituent as shown Fig. 9. Therefore, low-melting eutectic constituents were largely formed at the grain boundary during solidification, and the cracking propensity increased.

3.5. Solidification temperature range

The solidification temperature range is also a primary factor that controls solidification cracking resistance. The effect of the solidification temperature range can be found by the size of the solid + liquid (mushy) zone. During welding, the mushy zone that is susceptible to cracking under the influence of restraint trails behind the liquid weld pool. The formation of low-melting eutectic constituents at the last stage of solidification widen the solidification temperature range and increases the cracking tendency by expanding the crack susceptible mushy zone.

Table 3. The composition of g matrix and g/Laves eutectic phase in Inconel 625 and 718 overlays (unit: wt.%)

		Ni	Cr	Fe	Nb	Mo	Ti
Inconel 625 D10	Dendrite core	65.71	20.35	2.53	2.35	7.36	0.13
	γ/Laves	49.73	16.07	1.72	16.52	14.00	0.22
Inconel 625 D20	Dendrite core	67.67	21.48	2.29	2.14	5.89	0.53
	γ/Laves	51.22	16.81	2.01	14.53	14.45	0.98
Inconel 625 D30	Dendrite core	68.01	21.14	2.21	2.21	5.73	0.70
	γ/Laves	51.89	17.57	1.97	13.65	13.67	1.25
Inconel 718 D10	Dendrite core	56.90	19.44	17.60	2.89	2.30	0.87
	γ/Laves	45.02	12.24	10.77	24.95	5.47	1.55
Inconel 718 D20	Dendrite core	59.37	19.45	15.21	2.68	2.14	1.15
	γ/Laves	46.38	12.75	10.85	22.87	5.56	1.59
Inconel 718 D30	Dendrite core	63.82	18.96	11.97	2.35	1.60	1.30
	γ/Laves	48.88	13.60	9.45	21.31	4.87	1.89

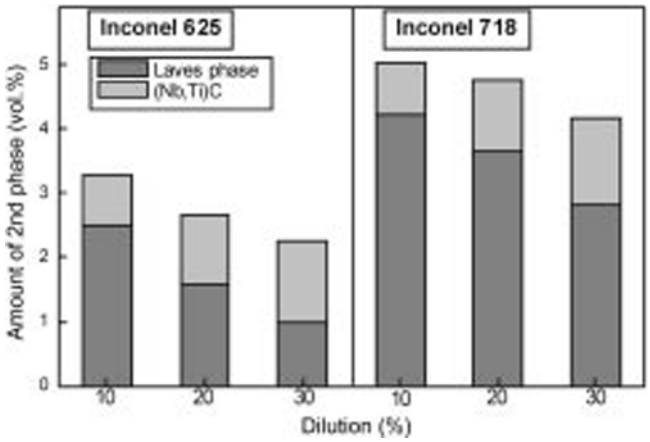

Fig. 8. Variation in total eutectic constituents, γ/NbC and γ/Laves with dilution.

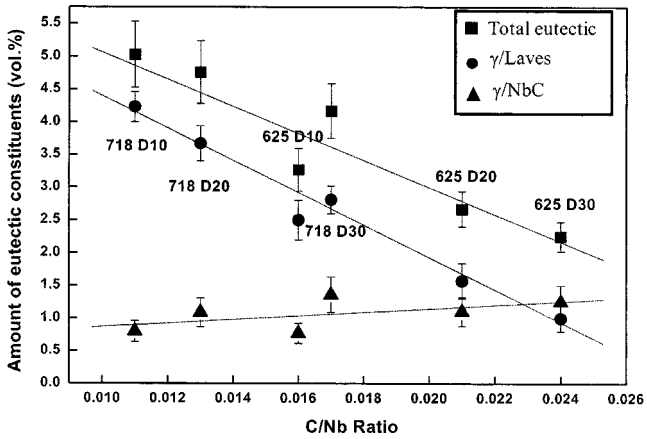

Fig. 9. The change in amount of eutectic constituents with C/Nb ratio.

Table 4. The C/Nb ratio and the amount of eutectic constituents for Inconel 625 and 718 overlays (unit: wt.%)

	C/Nb ratio	Amount of eutectic constituents (vol.%)		
		Total eutectic	γ/NbC	γ/Laves
Inconel 625 D10	0.016	3.27	0.77	2.50
Inconel 625 D20	0.021	2.67	1.10	1.57
Inconel 625 D30	0.024	2.25	1.25	1.00
Inconel 718 D10	0.011	5.03	0.80	4.23
Inconel 718 D20	0.013	4.76	1.09	3.67
Inconel 718 D30	0.017	4.17	1.36	2.81

Fig. 12 presents the DSC cooling curves acquired on Inconel 625 and 718, respectively. The DSC thermograms for the alloys exhibit a large exothermic peak which is associated with the formation of the primary γ dendrites. And two secondary peaks associated with the formation of γ/NbC and γ/Laves eutectic constituents, respectively. The solidification temperature range was represented as DT and this is

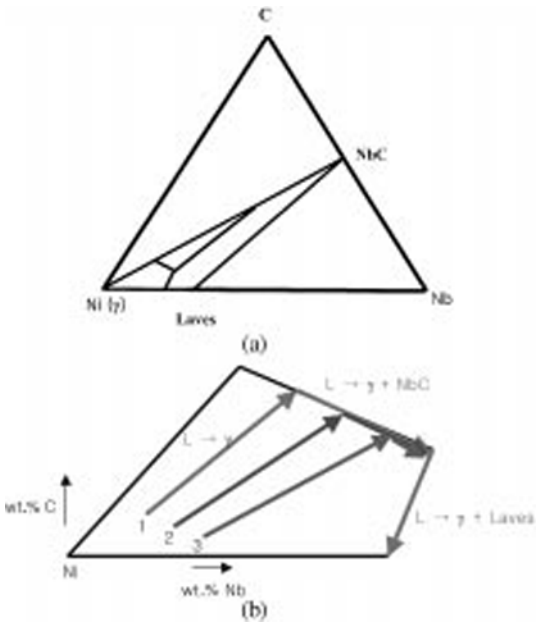

Fig. 10. (a) The liquidus projection for Ni-Nb-C and (b) the solidification paths with C/Nb ratio.

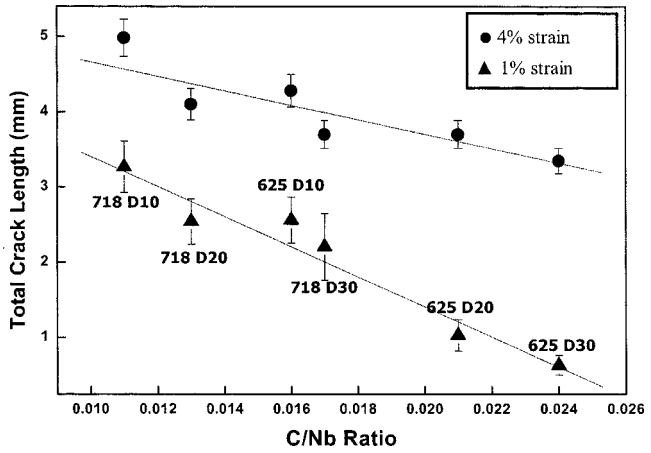

Fig. 11. Effect of C/Nb ratio on the total crack length as a function of the C/Nb ratio.

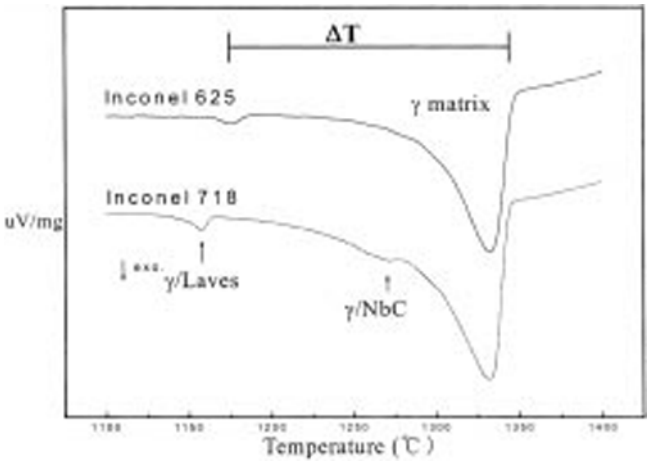

Fig. 12. Typical DSC solidification scans for Inconel 625 and 718.

calculated by the temperature difference between the α matrix formation and α/Laves formation. In two alloys, solidification temperature expanded to a lower temperature due to the formation of the γ/Laves eutectic constituent. The temperature of the secondary solidification reactions in the Inconel 625 and 718 overlays are presented in Table 5. As dilution increased in each overlay, the γ/Laves formation temperature moved to higher temperature. In Table 3 and Fig. 10, the amount of Nb required in the formation of γ/Laves is lowered with increasing dilution. So the formation of γ/Laves occurred at higher temperature. Thus, as the dilution increased, the solidification temperature range (DT) decreased. The Inconel 718 overlay was expected to have a higher cracking propensity than the Inconel 625 overlay because of the large solidification temperature range. Fig. 13 plots the maximum crack length as a function of the solidification temperature range (DT). As the solidification temperature range increased, the maximum crack length increased proportionally.

Table 5. Summary of secondary solidification reaction temperature in Inconel 625 and 718 overlays (unit: °C)

	γ matrix	γ/NbC	γ/Laves	ΔT
Inconel 625 D10	1352	1311	1206	146
Inconel 625 D20	1348	1314	1244	104
Inconel 625 D30	1345	1327	1297	48
Inconel 718 D10	1352	1308	1192	164
Inconel 718 D20	1352	1273	1204	148
Inconel 718 D30	1351	1330	1216	135

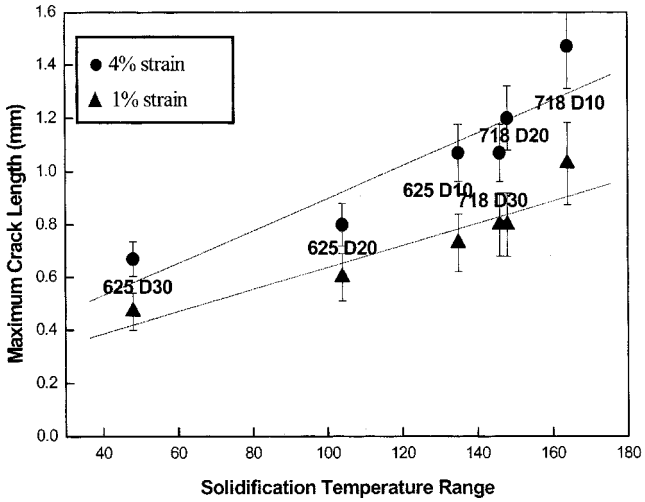

Fig. 13. Effect of C/Nb ratio on the maximum crack length as a function of the C/Nb ratio.

3.6. Fractography

Solidification cracking of the Inconel 625 and 718 overlay deposits was associated with the significant partitioning of Nb, Mo and Ti to the interdendritic and grain boundary regions. The segregation of these elements promoted the formation of low melting eutectic constituents (γ/NbC and γ/Laves) in the grain boundaries. Therefore, solidification cracking occurred along these grain boundaries decorated with the eutectic constituents, especially, the γ/Laves constituent.

A typical solidification crack surface is presented in Fig. 14. Fig. 14(a) shows dendritic appearance at the region of crack initiation. This dendritic crack surface indicates the existence of liquid during crack opening. These dendritic appearing fracture surfaces gradually disappeared with crack propagation (Figs. 14(b) and (c)). However, it is clear that the grain boundary was liquated. Thus, the solidification cracks propagated along the grain boundaries were embrittled by low melting constituents (γ/NbC and γ/Laves).

4. CONCLUSION

1. The solidification cracking of Inconel 625 and 718 overlay deposits were closely related with the γ/NbC and γ/Laves

Fig. 14. The Solidification crack surfaces in Inconel 718 compared with crack propagation.

eutectic constituents formed along the grain boundaries.

2. Minor variations in the Nb, Mo and Ti content have a strong influence on the solidification temperature range, type and amount of eutectic phases formed during solidification

3. As the dilution increased, C/Nb ratio increased and the amount of eutectic phases decreased. So the total crack length of overlay deposits decreased.

4. As the dilution increased, the solidification temperature range decreased and the maximum crack length of the overlay deposits decreased. Therefore, as the dilution increased, the solidification cracking propensity decreased.

5. The Inconel 718 overlay deposits had a higher cracking propensity than Inconel 625 overlay because of the larger amount of eutectic phases formed along with the wider solidification temperature range

ACKNOWLEDGMENT

This study was conducted with the support for specific foundation research (project number: A00-982-1104-03-2-2) of the Ministry of Commerce, Industry and Energy (MOCIE) of the Republic of Korea.

REFERENCES

1. T. Moriyama, Y. Izaki, K. Umeda, R. Oka, Y. Nishioka, and T. Tanaka, *Mater. Sci. Tech.* **10**, 993 (1994).
2. J. R. Nicholls, *Mater. Sci. Tech.* **10**, 1002 (1994).
3. J. R. Nicholls, *Mater. High Temp.* **12**, 35 (1994).
4. K. Easterling, *Introduction to the Physical Metallurgy of Welding*, p.164, Butterworths (1983).
5. H. B. Kim and C. H. Lee, *J. KWS*, **15**, 79 (1997).
6. H. B. Kim and C. H. Lee, *J. MRS* **7**, 162 (1997).
7. J. N. DuPont, C. V. Robino, and A. R. Marder, *Welding J.* **10**, 417s (1998).
8. J. N. DuPont, C. V. Robino, and A. R. Marder, *Acta mater.* **46**, 4781 (1998).
9. J. N. DuPont, C. V. Robino, J. R. Micheal, M. R. Notis, and A. R. Marder, *Metall. Trans. A* **29**, 2785 (1998).
10 .J. N. DuPont, C. V. Robino, J. R. Micheal, M. R. Notis, and A. R. Marder, *Metall. Trans. A* **29**, 2797 (1998).
11. M. J. Cieslak, T. J. Headley, G. A. Knorovsky, A. D. Romig, Jr, and T. Kollie, *Metall. Trans. A* **21**, 479 (1990).
12. C. D. Lundin and C. H. Lee, *Proc. of the JDC University Research Symp.*, p.33, Int. Welding Congress, ASM (1985).
13. S. C. Ernst W. A. Baeslack, and J. C. Lippold, *Welding J.* **10**, 418s (1989).
14. M. C. Maguire and J. R. Michael, *Superalloys 718, 625, 706 and Various Derivatives*, p. 881, TMS (1994).
15. B. Radhakrishnan and R. G. Thompson, *Metall. Trans. A* **20**, 2866 (1989).